Engineering Properties of Limestone Calcined Clay Concrete

Quang Dieu Nguyen, Mohammad Shakhaout Hossain Khan and Arnaud Castel

Related Papers Click to Download full PDF!

Click to Submit your Papers

Scientific paper

Engineering Properties of Limestone Calcined Clay Concrete

Quang Dieu Nguyen[1]*, Mohammad Shakhaout Hossain Khan[2] and Arnaud Castel[3]

Abstract

In this paper, various engineering properties of both fresh and hardened concrete with various limestone and calcined clay contents are investigated. Two concrete grades were considered: 50 MPa or 30 MPa average 28 days compressive strength. A low grade calcined clay was used with about 50% amorphous phase.
A reduction in concrete workability was observed with the increase in General Purpose (GP) cement substitution. Superplasticiser was required to obtain a slump equivalent to that of reference GP cement concrete. With 15% GP cement replacement rate, the 28 days compressive strength achieved was superior to that of reference grade 50 MPa concrete, reaching 58 MPa. However, the average 28 days compressive strength reduced significantly with 30% and 45% GP cement replacement, reaching about 35 MPa. Considering concretes with similar 28-day compressive strength, results showed that the 7-day compressive strength was only marginally affected by the limestone and calcined clay substitution. Mercury intrusion porosimetry results revealed that incorporating calcined clay and limestone led to significant refinement of the porosity: increase in the quantity of pores inferior to $0.01\,\mu m$ and reduction in the quantity of coarse pores (with size $> 0.1\ \mu m$).

1. Introduction

The production of Portland cement takes responsibility for 5% to 7% of the worldwide man-made CO_2 emission, of which 50% is from the chemical process and 40% from burning fuel (Damtoft *et al*. 2008; Worrell *et al*. 2001). The utilization of supplementary cementitious materials (SCMs), such as fly and Ground Granulated Blast Furnace Slag (GGBFS) which allows to decrease the quantity of Portland cement used in concrete, has been a rational approach to reduce the overall carbon footprint of construction industry.

Among promising SCMs, calcined clays have received a considerable attention nowadays due to their global availability. Clay structure is a combination of silica and alumina sheets and alumina-silicates minerals representing 74% of the earth's crust. Clay is available almost everywhere (Antoni 2013), whereas supply of traditional SCMs (fly ash or GGBFS) is only limited to some areas of the world (Damtoft *et al*. 2008). Using calcined clay allows eventually to improve the pore

[1]PhD Candidate, Centre for Infrastructure Engineering and Safety, School of Civil and Environmental Engineering, The University of New South Wales, Sydney, NSW 2052, Australia. *Corresponding author, *Email:* qd.nguyen@unsw.edu.au
[2]Research Associate, Centre for Infrastructure Engineering and Safety, School of Civil and Environmental Engineering, The University of New South Wales, Sydney, NSW 2052, Australia.
[3]Associate Professor, Centre for Infrastructure Engineering and Safety, School of Civil and Environmental Engineering, The University of New South Wales, Sydney, NSW 2052, Australia.

structure of concrete as a result of pozzolanic reactions between AS_2 ($Al_2O_3.2SiO_2$) and CH (Siddique and Klaus 2009). However, similarly to fly ash and GGBFS, calcined clay has a negative impact on the early age strength development of mortar and concrete. As a result, Portland cement concrete containing SMCs generally shows a decline in strength at early age and similar or greater strength at later age (Lothenbach *et al*. 2011; Menendez *et al*. 2003).

A possible approach to address this problem is the addition of limestone in ternary blended cement. Limestone powder provides an increase of the surface area for the nucleation of hydration products, leading to an acceleration of reactions, which is known as filler effect. Previous studies utilized isothermal calorimetry and compressive strength test to highlight the positive "filler effect" of finely powdered limestone in different particle size and OPC replacement rates (Kumar *et al*. 2013a; Kumar *et al*. 2013b; Oey *et al*. 2013). Beside the physical filler effect, limestone also acts as an accelerator for alite hydration resulting in the improvement of the early strength (Damtoft *et al*. 2008). Moreover, calcium carbonates of limestone powder can interact with aluminate hydrates, leading to the stabilization of ettringite and an increase in the total volume of hydration products. This reaction can be limited due to a lack of aluminate content in anhydrous clinkers. However, even when sufficient and highly reactive alumina are provided in the system such as hydratable alumina, the generation of carbonate-AFm is limited by the low dissolution rate of limestone (Puerta-Falla *et al*. 2015a; Puerta-Falla *et al*. 2015b). Moreover, highly soluble carbonate salts (Na_2CO_3) fail to enhance the formation of carboaluminate phases in hydration products, which indicates the essential role of calcium in carboaluminate phases formation (Puerta-Falla *et al*. 2016) . However,

in some extent, SCMs with high alumina content can produce significant amount of carboaluminate phases if blended with a large amount of limestone (De Weerdt *et al.* 2011; Matschei *et al.* 2007). As a result, a consolidation of SCMs and limestone in ternary blended cement can provide a blend with sufficient development in strength, since limestone filler governs the early strength and SCMs provide the long-term strength. Various studies have been conducted to investigate ternary blended cements containing limestone. Mounanga (Mounanga *et al.* 2011) stated that mechanical strength of ternary binder (OPC – fly ash – limestone) was higher than that of the binary binder, for a constant cement substitution rate. Another author (De Weerdt *et al.* 2011) also found that 5% of OPC or fly ash can be replaced by limestone without affecting the concrete compressive and tensile strengths. All results revealed that limestone powder can prevent the reduction in early age strength of concrete containing SCMs.

The synergy between calcined clays and limestone powder in ternary blended cement has also been considered. Antoni (Antoni *et al.* 2012) showed that a ratio of 2 : 1 of metakaolin and limestone powder provided better mechanical properties at 7 and 28 days than that of 100% OPC concrete for OPC replacement rates up to 45%. The reaction between calcium carbonates and aluminates produced supplementary AFm phases (hemi-carboaluminate) and stabilized ettringite. The results also revealed that calcined clay reacted more efficiently together with limestone in a ternary system than in a binary blend of calcined clay and OPC. Another investigation (Tironi *et al.* 2017) utilized a 3 : 1 proportion of kaolinitic calcined clay and limestone filler looking at OPC replacement rates up to 40%. Results revealed that limestone filler facilitates pozzolanic reactions particularly at early age leading to a significant reduction in the quantity of coarse pores in the matrix. Another author (Shi *et al.* 2017) investigated the resistance of calcined clay and limestone mortars against sulphate attack, chloride diffusion and carbonation. Metakaolin-limestone mortars exhibited a high resistance against chloride and sulphate attack but a poor performance against carbonation compared to reference OPC mortar. OPC reference mortars showed the highest resistance to carbonation while both binary blend with metakaolin and ternary blend with metakaolin and limestone revealed a lower resistance. Limestone mortar was the most vulnerable to carbonation (Khan *et al.* 2018; Shi *et al.* 2016). Recently, Kunther (Kunther *et al.* 2016) reported that blending metakaolin with limestone leads to the suppression of stratlingite and other phases such as monoslfate, hemicarbonate and monocarbonate. Another author (Vance *et al.* 2013a) observed a reduction in Portlandite content due to the pozzolanic reactions and the formation of carboaluminate hydrates, confirmed by DTG analysis.

Limestone calcined clay cement (LC3) (Antoni *et al.* 2012) is a new and promising environmental-friendly and low embodied carbon cement. However, numerous engineering properties of LC3 concrete must be assessed before adoption by the industry. In this paper, limestone and calcined clay (with a ratio of 2 : 1) were blended with General Purpose (GP) cement. The GP cement substitution rates considered were 15%, 30% and 45%. Limestone and calcined clay blend is used as any other SCM in Australia by straight replacement of GP cement in the concrete mix without any optimisation of sulphate content or alkalinity of the blended cement (Antoni *et al.* 2012). A low grade calcined clay was used with about 50% amorphous phase. Indeed, studies focusing on pure grade kaolinite clays overlook the potential application of large-scale availability of low-grade calcined clays (Badogiannis *et al.* 2005; San Nicolas *et al.* 2013; Tironi *et al.* 2013). In this study, performance-based approach is adopted in order to determine the suitability of limestone calcined clay-based concrete for structural applications. Various engineering properties of both fresh and hardened concrete with various limestone and calcined clay contents are investigated including workability, mechanical properties, bulk density, pulse velocity and drying shrinkage. Moreover, some durability related properties such as surface resistivity, porosity, pH and pore solution compositions were thoroughly assessed. Finally, X-ray diffraction was used to identify the crystalline phases produced. The performance of limestone calcined clay-based concrete is compared to that of reference GP cement concrete.

2. Experimental program

2.1 Materials
The limestone calcined clay cement concrete used in the study is a ternary blend of General Purpose (GP) cement, calcined clay and limestone. All raw materials were obtained from the industry. The GP cement complies with the Australia Standard AS 3792-2010. Importantly, Portland cement content is about 90% in Australian GP cements. Indeed, 7% to 8% of mineral additions are allowed in GP cement in addition to 2% to 3% of gypsum. Limestone and calcined clay blend are used as any other SCM in Australia by straight replacement of GP cement in the concrete mix without any optimisation of sulphate content or alkalinity of the blended cement (Antoni *et al.* 2012). This approach aims to reduce the time for limestone and calcined clay blend adoption in the industry. The limestone branded as Stone Dust was supplied by Boral Construction Materials Limited in New South Wales, Australia. The calcined clay used was made using a flash calcination process and supplied by Argeco, France. **Table 1** shows the chemical composition of all cementitious materials determined by X-ray fluorescence (XRF) and the mineralogical composition of GP cement determined by using XRD-Rietveld analysis. XRD patterns of the calcined clay and the limestone are presented in **Fig. 1**. The only crystalline phases identified are quartz in the calcined clay and calcite in the limestone.

Table 1 Chemical Composition of Cementitious Materials and the Mineralogical Composition of GP Cement.

Chemical composition	GP cement (wt.%)	Calcined clay (wt.%)	Limestone (wt.%)	Cement mineralogical composition (wt.%)	
SiO_2	19.74	70.42	0.36	C_3S	51.2
Al_2O_3	4.70	22.34	0.11	C_2S	16.5
Fe_2O_3	2.98	2.34	0.1	C_3A	6.5
CaO	64.62	0.49	57.51	C_4AF	7.3
MgO	1.48	0.16	0.29		
Na_2O	0.21	0.1	-		
K_2O	0.64	0.19	-		
TiO_2	0.31	1.1	-		
SO_3	2.24	0.02	-		
Loss on ignition (LOI)	3.18	1.76	42.61		

Calcined clay and limestone were analysed using a Hitachi S-3400N scanning electron microscope (SEM) at Mark Wainwright Analytical Centre, UNSW Sydney,
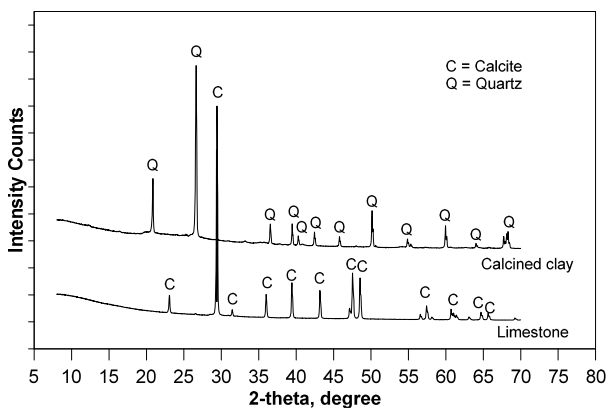

Fig. 1 XRD patterns of metakaolin and limestone.

Australia (**Fig.2**). Gold coating was applied into samples prior to the analysis. The system configuration for SEM analysis comprised working voltage of 20 kV, probe current of 50 and working distance of 10 mm. The presence of spherical particles (**Fig. 2(a)**) with agglomerated particles of metakaolin on its surface (**Fig. 2(b)**) represents the main disparity between flash calcined clay and traditional calcined clay. Indeed, traditional calcined clay is mostly composed of few nanometres thick hexagonal particles. During the flash calcination, the clay melts in a hot gas steam, creating a significant quantity of spherical particles. Similar morphology can be noticed in other SCMs such as fly ash (San Nicolas *et al.* 2013). Argeco calcined clay can contain 10 to 15% of spherical particles (Cassagnabere *et al.* 2013; San Nicolas *et al.* 2013). The particle size distribution and characteristics of GP cement, calcined clay and limestone powders are presented in **Fig. 3** and **Table 2**,

(a) Calcined clay
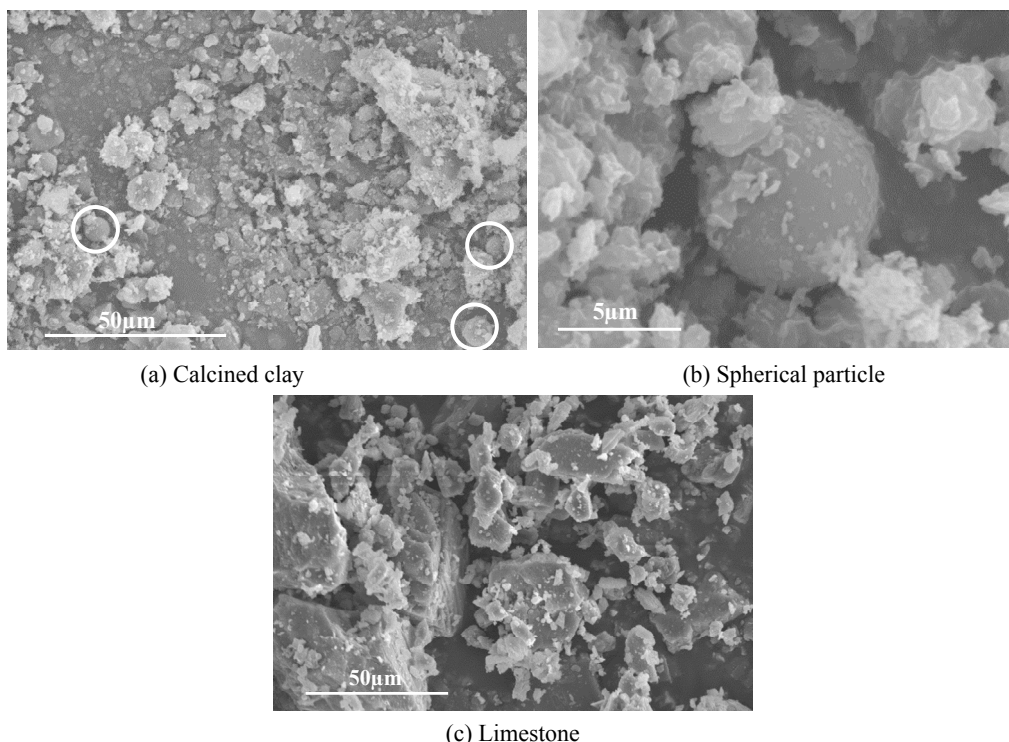

(b) Spherical particle

(c) Limestone

Fig. 2 SEM images of calcined clay and limestone.

Table 2 Results from particle size distribution measurement.

Material	Particle Size Distribution [μm]		
	D_{v10}	D_{v50}	D_{v90}
GP cement	1.32	8.48	25.26
Calcined clay	2.50	21.19	64.75
Limestone	7.74	43.35	130.46

respectively. Laser diffraction technique by Malvern Mastersizer 2000 instrument measuring particle sizes ranging from 0.01 μm to 10 mm was used to determine the particle size distribution (PSD). GP cement was dispersed into isopropanol to prevent any hydration whilst calcined clay and limestone were dispersed into water and ultrasonic was utilized to scatter powders into primary particles. GP cement showed the finest PSD and limestone had a significantly higher percentage of coarse particles with a D_{v90} being around 130 μm. Calcined clay and limestone used are classified as coarse calcined clay and coarse limestone, respectively, based on previous studies (Bosiljkov 2003; Vizcaíno Andrés *et al.* 2015).

The selection of calcined clays to be used as SCM is mainly based on their reactivity which is governed by the transformation of the kaolinite during the calcination process (San Nicolas *et al.* 2013; Tironi *et al.* 2012). XRD results revealed that there is no trace of kaolinite in the calcined clay (**Fig. 1**), which indicates that all the kaolinite was dehydroxylated during calcination. The dehydroxylation of kaolinite results in the formation of amorphous material with high reactivity in cement-based system (He *et al.* 1995; San Nicolas *et al.* 2013; Tironi *et al.* 2012). The quantity of amorphous phases after the calcination process is an important factor as well. The amorphous content of the calcined clay used in this study is 50.9%, obtained from XRD-Rietveld refinement (**Table 3**), which classifies this calcined clay as low-grade (Badogiannis *et al.* 2005; Badogiannis *et al.* 2004; Badogiannis and Tsivilis 2009; Vizcaíno *et al.*

Table 3 Mineral composition of calcined clay determined by XRD-rietveld analysis.

Minerals	[wt.%]
Quartz	49.1
Amorphous	50.9

2015). XRD-Rietveld results are consistent with the high silicon dioxide content obtained by XRF analysis (**Table 1**). Indeed, **Table 1** shows that the SiO_2 content represents over 70% of the total weight of calcined clay and the SiO_2/Al_2O_3 molar ratio is 5.3, which is higher than that of kaolinite ($SiO_2/Al_2O_3 = 2$) due to the presence of quartz in large quantity. Calcined clay with high amorphous phase (over 90%) typically contains 50 - 55% SiO_2 and 40 - 45% Al_2O_3. In conclusion, an increase in silicon dioxide content with a decrease in aluminum oxide content reflect a decrease in amorphous phase (Badogiannis *et al.* 2005; Ramezanianpour 2014; San Nicolas *et al.* 2013; Tironi *et al.* 2012).

Fine aggregate is Sydney sand with a specific gravity of 2.65 and water absorption of 3.5%. Crushed basalt supplied from Dunmore quarry in New South Wales, Australia was utilized as coarse aggregate. Its characteristics comprised specific gravity of 2.8, maximal nominal size of 10 mm and water absorption of 1.6%. To obtain saturated surface dry (SSD) condition, all aggregates were first oven dried at 105°C for 24 h to eliminate any moisture content, then the exact amount of water required was added prior to concrete casting.

2.2 Concrete mix design and batching procedure

Two concrete grades were considered with an average 28 days compressive strength superior to 50 MPa or 30 MPa. Five concrete mixes have been fabricated. Two reference concretes using only GP cement, labelled GPC-30 and GPC-50 and three LC3 concretes labelled LC3-15, LC3-30 and LC3-45. The LC3-15, LC3-30 and LC3-45 mixtures are defined by the rate of GP cement
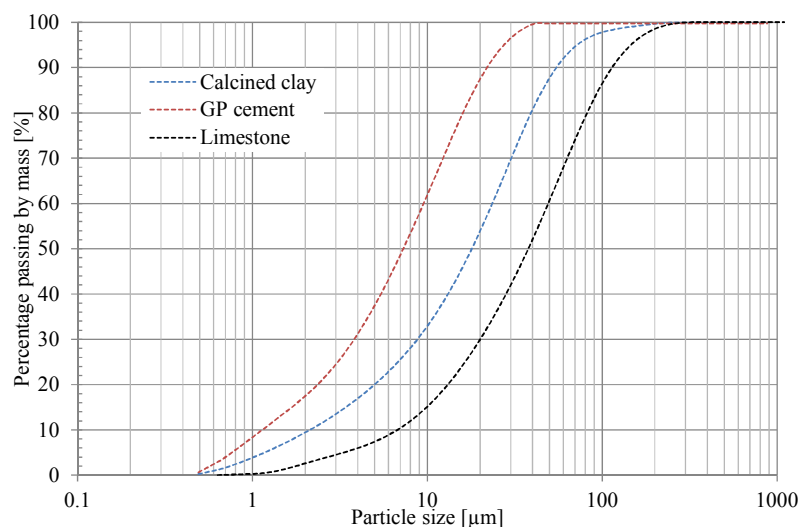
Fig. 3 Particle size distribution of GP cement, calcined clay and limestone.

Table 4 Mix design details of concretes.

Materials (kg/m^3)	GPC-30	GPC-50	LC3-15	LC3-30	LC3-45
Coarse aggregate	1265	1221	1221	1221	1221
Fine aggregate	545	620.8	620.8	620.8	620.8
Total binder	380	388	388	388	388
GP cement	380	388	329.8	271.6	213.4
Calcined clay	0	0	38.8	77.6	116.4
Limestone	0	0	19.4	38.8	58.2
Water/binder ratio	0.55	0.45	0.45	0.45	0.45
Water	210	174.5	174.5	174.5	174.5

replacement being 15%, 30% and 45% with the ratio 2 : 1 by mass of calcined clay and limestone. However, as mentioned previously, Australian GP cements contain about 90% of OPC. As a result, the OPC content of LC3-15, LC3-30 and LC3-45 binders is about 76.5%, 63% and 49.5% respectively. All mix designs are given in **Table 4** with aggregate mass in saturated surface dry (SSD) condition. All concretes have very similar binder content and water to binder ratio except for GPC-30. The GPC-30 mixture was designed to achieve a 28 days average compressive strength similar to that of LC3-30 and LC3-45. Then, transport and durability properties of concrete could be compared between concretes with similar mechanical properties (see section 3).

Fresh properties of concrete were measured during concrete batching period. After measuring fresh concrete properties, concrete was poured into the moulds and a vibrating table was used to compact the concrete. Two kinds of moulds were utilized including cylinder with 100 mm diameter and 200 mm height together with rectangular prisms with the dimension of 75 mm × 75 mm × 285 mm used for shrinkage tests only. After surface finishing, all moulds were covered by using lids to prevent surface from moisture loss.

2.3 Curing condition
All concrete specimens were demoulded after one day. Then, all specimens were placed into a lime-saturated water bath (by dissolving an excess of calcium hydroxide in distilled water) continuously for 7 days and room temperature of 23 ± 2°C. After that, the specimens were stored in the controlled room at a fixed temperature of 23 ± 2°C and relative humidity (RH) of 50% until the testing dates.

2.4 Testing program
(1) Fresh concrete properties
Slump test to determine concrete workability was carried out according to AS1012.3.1 (ASTM C143) while density of fresh concrete (mass per unit volume) was measured in accordance with AS1012.5 which is similar to ASTM C138.

(2) Mechanical properties
The compressive strength was measured at 7, 14, 21 and 28 days using three 100 mm diameter standard cylinders following standard AS1012.9 (ASTM C39). The modulus of elasticity and splitting tensile strength were

measured using three duplicates at 28 days in accordance with AS1012.17 and AS1012.10 (ASTM C469 and ASTM C496), respectively.

(3) Other physical properties
The ultrasonic pulse velocity (UPV) of concrete was evaluated in accordance with ASTM C597. Cylindrical samples with 200 mm in height and 100 mm in diameter were used. Prior to measuring the pulse of ultrasonic wave, petroleum jelly used as coupling agent was applied to all the transducers faces as well as sample surfaces to ensure efficient movement of energy between concrete and transducers. The coupling agent is able to remove any entrapped air on the connecting surface between the transducers and specimens. An insufficient and inappropriate agent can generate incorrect values of time measurement. The pulse velocity was determined as following: V = L/T where V is pulse velocity in m/s, L is the gap between centres of transducer faces in m and t is transit time in s.

Surface resistivity measurement based on AASHTO TP95 was performed by utilizing a 4-pin Wenner probe array. Water-saturated 100 × 200 mm cylinders 28 days of age were used. A current flow in samples was generated by an alternating current potential divergence at the outer pins of the Wenner array. The resultant potential difference between the two inner pins was monitored. The current and resultant potential was used to quantify the surface resistivity magnitude. The bulk density of hardened concrete was measured using 100 mm diameter discs with 50 mm height, which was cut from the standards cylinders and test protocol was following ASTM C642.

The pore structure of pastes was analysed by mercury intrusion porosimetry (MIP) which was conducted at Particle & Surface Sciences Pty. Limited, Sydney, Australia by using AutoPore IV 9500 V1.09. MIP experiment was conducted after 28 days. Five specimens of approximately 5 mm size with a total mass of 3 g were collected and immersed into isopropanol to stop hydration (Zhang and Scherer 2011). After 7 days of immersion, the specimens were dried using vacuum desiccator for 7 days before testing. MIP analysis utilized contact angle of 130° and surface tension of 0.485 N/m with a maximum pressure to 400 MPa.

Drying shrinkage of LC3 concrete was measured using prism specimens with dimension of 75 × 75 × 285 mm. The drying shrinkage was calculated over a 250

Table 5 Fresh concrete properties.

Concrete type	Slump (mm)		Fresh density (kg/m^3)	Superplasticizer (% by weight of cement)
	Without superplasticiser	With superplasticiser		
GPC-30	180	-	2382	-
GPC-50	140	-	2353	-
LC3-15	70	130	2440	0.38
LC3-30	50	170	2379	0.85
LC3-45	25	180	2344	1.23

mm gauge length. The fabrication of shrinkage specimens and the measurement protocol of drying shrinkage followed the standards AS 1012.8.4 and AS 1012.13 which are similar to ASTM C157 and ASTM C490, respectively.

(4) The pH and pore solution composition

To measure the pH of the pore solution, cylindrical specimen with dimensions of 50 mm diameter and 100 mm height were cast with LC3 pastes having the same mix design and curing condition as the LC3 concretes. To prevent ions leaching during the curing period, the first day, the specimens were stored in the cylindrical plastic moulds with a lid in a controlled room at 23 ± 2°C and 50% RH. The specimens were then demoulded and placed in containers with airtight lids. The air-tight containers were filled with lime-saturated water up to about 10 mm to maintain a saturated condition. The perforated racks were utilized to prevent the contact between specimens and lime-saturated water. The containers were continuously stored in the controlled room at temperature at 23 ± 2°C and 50% RH until 7 days. Subsequently, specimens were removed from the containers and placed in the 23 ± 2°C and 50% RH room until 28 days. This curing process has been successfully utilized in a previous study for pore solution analysis (Kim *et al.* 2015). Pore water was then extracted according to well established method proposed by Barneyback and Diamond (1981). The pH of the extracted pore solution was directly measured by using a calibrated pH probe. Furthermore, the ion concentration in the extracted pore water was measured by using Inductively Coupled Plasma Optical Emission spectroscopy (ICPOES). Pore water was diluted with deionized water and analysed by Perkin Elmer OPTIMA 7300 ICP Optical Emission Spectrometers and obtained results were corrected by dilution factor.

(5) Identification of crystalline phases

The crystalline phases in LC3 samples were identified by using X-ray diffraction (XRD). 50 mm cube specimens of LC3 pastes were used having the same mix design and similar curing conditions as LC3 concretes. The paste samples were ground to powder which was then analysed using X-ray diffractometer Phillips X'Pert Pro Multi-purpose (MPD) system housed at the Mark Wainwright Analytical Centre at the University of New South Wales, Australia. This used Cu-Kα radiation with a wavelength of 0.15418 nm and operated at 45 kV and 40 mA, scan range 5 - 65° and 0.026° 2θ step size. The

scan results were interpreted using the software package HighScore Plus for phase identification.

3. Results and discussions

3.1 Fresh concrete properties

Slump and fresh density of the mixtures are presented in **Table 5**. The slump of GPC-30 was the highest due to its highest water to binder ratio or the highest amount of water in mix design compared to other concretes. For LC3 concrete, a reduction in workability was observed with the increase in GP cement substitution. The addition of calcined clay and limestone adversely affects the rheology of the mix. To be more specific, GPC-50 and GPC-30 obtained 140 mm and 180 mm of slump respectively whereas slump values reduced remarkably to 70, 50 and only 25 mm for LC3-15, LC3-30 and LC3-45 respectively. Superplasticiser dosage in the range of 0.38 to 1.23% was used, resulting in a significant improvement in workability for all LC3 mixes with slumps ranging from 130 to 180 mm. Preliminary study reported that coarse limestone could decrease the yield stress and plastic viscosity of pastes due to an increase in particle spacing (Vance *et al.* 2013b). However, the positive effect of coarse limestone could not compensate the negative impact of the substantial calcined clay content. The potential for agglomeration of metakaolin particles leads to de-watering in the fresh mixture (Ambroise *et al.* 1994; Vance *et al.* 2013b), which causes a remarkable escalation in the yield stress and plastic viscosity and then a reduction in workability.

In comparison with calcined clay from traditional calcination, using flash calcined clay allows to limit the loss in workability of fresh concrete (San Nicolas *et al.* 2013; San Nicolas *et al.* 2014). For example, 180 mm of slump was achieved by using only 1.23% of superplasticiser for LC3-45 concretes in this study while Wild (Wild *et al.* 1996) used up to 3.6% of superplasticiser to obtain only a moderate slump (90 mm) for specimens containing 30% metakaolin. The difference is attributed to the significant amount of spherical particles in flash calcined clay (**Fig. 2**) which are not observed in soak or rotary kiln calcined clay (Cassagnabere *et al.* 2013; San Nicolas *et al.* 2013; San Nicolas *et al.* 2014). Another reason why the flash calcined clay used in this study has less impact on workability compared to results reported by other authors is the large amount of quartz (49.1%) in its mineral composition. Indeed, pure metakaolin with much higher amorphous phase content can reduce further the workability of fresh concrete, which makes it

Table 6 pH and pore solution compositions of cement pastes at 28 days.

Concrete type	pH	Ca (mg/L)	Na (mg/L)	Mg (mg/L)	K (mg/L)	Al (mg/L)	Si (mg/L)	Ti (mg/L)	S (mg/L)
GPC-30	13.48	81.0	858	0	9162	1.08	0	0.002	48.0
GPC-50	13.35	76.5	1831	0	6929	1.26	3.06	0.06	209
LC3-15	12.91	41.8	1304	0.01	4564	31.4	30.9	0.07	100
LC3-30	12.89	259	1799	0.02	2955	0.78	1.9	0.03	83.3
LC3-45	12.66	73.1	1236	0.02	1118	12.1	5.19	0.03	58.2

not always practical (Brooks and Johari 2001; Wild *et al*. 1996). Furthermore, there was no notable change in concrete fresh density for all mixes. The fresh density fluctuated between 2440 kg/m^3 and 2344 kg/m^3.

3.2 The pH and pore solution composition

Table 6 shows the pH and pore solution compositions of GP cement and LC3 pastes at 28 days. The composition of all pore solutions is dominated by Na, K, S and Ca. The pH reduces steadily when increasing the calcined clay and limestone content. This can be attributed to the reduction in total alkali metal (sodium and potassium) and hydroxide ions concentration due to the partial replacement of Portland cement and the decline in Ca(OH)$_2$ content due to the pozzolanic reactions. The reduction in GP cement dosage causes a decrease in alkali metal ions concentration such as Na and K. Indeed, the calcined clay and limestone blend is rich in silica and poor in alkalis. **Figure 4** shows a very good correlation between the reduction in sodium and potassium ions concentration in the pore solution and the rate of substitution of GP cement. **Table 6** shows that the sulphate concentration decreases drastically as well with the increase in GP cement substitution as sulphate ions are mainly derived from the gypsum in GP cement.

3.3 Identification of the crystalline phases in LC3 pastes

The XRD patterns of LC3 samples at 28 days are given in **Fig. 5**. Calcium silicate hydrate (C-S-H) phase was

found at 29.5°, 32° and 50°. Portlandite content is decreasing partially due to the pozzolanic reaction with calcined clay. However, the reduction in GP cement content in the mix with the increase of substitution by LC3 also contributes to the reduction in Portlandite observed.

The highest peak of calcite (CaCO$_3$) phase was found at 29.5°. CaCO$_3$ mainly comes from limestone as its composition includes 97% of calcium carbonate. Consequently, the higher amount of calcite was observed in the mixture with the higher GP cement substitution level. Similar tendency was observed for hemicarboaluminate phase. Hermicarboaluminate highest peak is around 10.7° and increases in magnitude from LC3-15 to LC3-45 concretes. The hemicarboaluminate phase is forming due to the hydration of calcium carbonate (Ipavec *et al*. 2011; Matschei *et al*. 2007). Hc is the dominant CO$_3$-AFm phase of LC3-based pastes, which is consistent with observations reported in previous studies when using metakaolin and excess limestone (Antoni *et al*. 2012; Puerta-Falla *et al*. 2015a; Puerta-Falla *et al*. 2015b). The absence of monocarboaluminate was observed at 28 days due to the slow dissolution rate of limestone. Indeed, the solubility and calcium content in carbonate source such as limestone in LC3 concrete govern in carboaluminate phase formation (Puerta-Falla *et al*. 2016).

Another crystalline phase which was also observed is quartz. This phase mainly derived from the calcined clay (**Table 1**). The highest peak of ettringite phase can
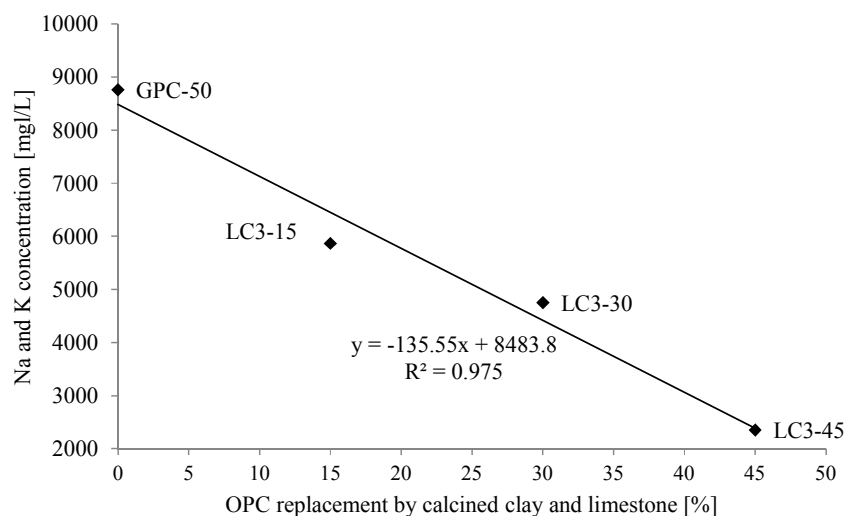

Fig. 4 Relationship between Na and K concentration in pore solution and the replacement of calcined clay and limestone content.

be found at 9.5° generally remaining stable among the three different LC3 concretes.

3.4 Mechanical properties of concretes

The compressive strengths including standard deviations of each data point from 7 to 28 days are given in **Fig. 6** for all concretes. After 28 days, LC3-15 samples obtained an average compressive strength of 58 MPa which was higher than that of reference concrete GPC-50. The 28-day compressive strength of LC3-30 and LC3-45 was 35.5 MPa and 36.3 MPa respectively, about 62% of LC3-15 compressive strength and similar to that of GPC-30. Considering concretes with similar 28-day compressive strength, results showed that the 7-day compressive strength was only marginally affected by the limestone and calcined clay substitution. After 14 days, the compressive strength of LC3 concretes is equivalent or higher than that of GPC-30 reference concrete.

Previous studies reported that LC3 mortars can develop a compressive strength higher or similar to Port-land cement reference mortar after 7 and 28 days with replacement rates up to 45% (Antoni *et al.* 2012; Shi *et al.* 2016). However, highly pure calcined clay with high amorphous phase content was used. Other authors, using low grade calcined clay (44% amorphous phase) (Tironi *et al.* 2017), reported that mortars with 20% replacement by mass of Portland cement could develop a similar compressive strength to reference mortar at 28 days but lower at 7 days. Moreover, compressive strength decreased noticeably in comparison with reference mortars at all ages for mortars with 40% substitution by mass of Portland cement. Those results are consistent with the results presented in **Fig. 6**. Quartz constitutes approximately 50% of the calcined clay used in this study, which is known as inert filler. Therefore, for high GP cement replacement rates, the synergy between calcined clay and limestone to form mono/hemicarboaluminate hydrates could not compensate the negative impact of the large amount of quartz, leading to a significant decrease in mechanical strength of LC3-30 and LC3-45 samples compared to LC3-15.

Fig. 5 XRD patterns of LC3 pastes at 28 days.

Fig. 6 Compressive strength development of concretes.

Another possible reason for the lower compressive strength of LC3-30 and LC3-45 samples is their low sulphate content compared to reference concretes and LC3-15. Indeed, the amount of sulphate is an important factor in the mechanical development of LC3 concrete since it facilitates the main silicate reactions in blended cement-based environment, especially in binder with 45% of replacement (Antoni *et al.* 2012). Previous study showed significant increase in compressive strength when adding extra gypsum up to 3% to the blend by enhancing C_3S hydration as well as increasing the amount of ettringite and hemicarboaluminate forming. In this study, GP cement was used without any addition of gypsum. As a result, the proportion of gypsum in LC3 binder declined with the increasing substitution. Therefore, specimens with high replacement rate (30% and 45% substitution) could have been subjected to sulphate depletion affecting the main silicate reaction and then the compressive strength of concrete. An optimisation of sulphate content and alkalinity (Antoni *et al.* 2012) could improve the performance of the concrete but this is not in the scope of this study which is looking at using limestone and calcined clay blend as any other SCM in Australia by straight replacement of GP cement.

Table 7 presents the modulus of elasticity and indirect tensile strength after 28 days. The elastic modulus of LC3-15 achieved 32.6 GPa, the highest value obtained. However, no clear trend in the development of the elastic modulus was observed for 30% and 45% replacement. To be more specific, the modulus of elasticity of LC3-30 sample declined to 29.3 GPa but the modulus of elasticity of LC3-45 raised to 30.7 GPa. The elastic modulus of GPC-30 was 28.6 GPa, which indicates that calcined clay and limestone are able to slightly improve the modulus of elasticity in comparison with GP cement concretes with the same compressive strength. Previous studies (Justice and Kurtis 2007; Khatib and Hibbert 2005; Qian and Li 2001) showed an increase in the elastic modulus associated with the utilization of calcined clay. However, another study (Bonavetti *et al.* 2000) reported that limestone addition caused a reduction in the elastic modulus. Consequently, the elastic modulus of LC3 concrete seems to be equivalent to that of reference GP cement concrete and does not correlate well with the alteration of the compressive strength observed.

The indirect tensile strength decreases only marginally with the increase in substitution. The indirect tensile strength of GPC-50 and GPC-30 were 4.6 MPa (which was the highest value) and 3.5 MPa respectively. The tensile strength reduced to 4.3 MPa for LC3-15 and 3.2 for LC3-30, the lowest indirect tensile strength, before increasing to 3.4 MPa in LC3-45 concrete.

3.5 UPV, Surface resistivity, bulk density and pore structure

Table 8 shows the ultrasonic pulse velocity (UPV), sur-

Table 7 Elastic modulus and indirect tensile strength of concretes at 28 days.

Concrete type	Modulus of elasticity (GPa)	Splitting tensile strength (MPa)
GPC-30	28.6 ± 0.7	3.5 ± 0.1
GPC-50	31.1 ± 0.9	4.6 ± 0.1
LC3-15	32.6 ± 1.2	4.3 ± 0.3
LC3-30	29.3 ± 1.0	3.2 ± 0.1
LC3-45	30.7 ± 0.9	3.4 ± 0.2

Table 8 Transport properties and bulk density of concretes at 28 days.

Concrete type	UPV (m/s)	Surface resistivity (kΩ.cm)	Bulk density (T/m^3)
GPC-30	4104	10.38	2.11
GPC-50	4508	19.4	2.25
LC3-15	4411	27.3	2.23
LC3-30	4320	48.2	2.20
LC3-45	4335	78.9	2.18

face resistivity and the bulk density of all concretes after 28 days. The pulse velocity reached the highest value of 4.5 km/s for GPC-50 specimens and decreased slightly when increasing the GP cement replacement with 4.4 km/s for LC3-15 and 4.3 km/s for both LC3-30 and LC3-45. The lowest value of UPV was 4.1 km/s for GPC-30 concrete. UPV values show that all LC3 concretes are of a good quality according to the classification proposed by Whitehurst (Whitehurst 1951). Compressive strength is considered closely correlated to pulse velocity (Lin *et al.* 2003; Sturrup *et al.* 1984). The pulse velocity of LC3-30 and LC3-45 are similar which is consistent with the similar values of compressive strength measured. The highest compressive strength at 28 days was measured on LC3-15 concrete whereas GPC-50 obtained the highest value of UPV, although the difference was not significant. The pulse velocity in concrete depends on numerous variables such as the elastic modulus of both aggregate and hardened cement paste, aggregate content, moisture condition etc (Lin *et al.* 2003; Neville 1995). Tharmaratram and Tan established a relationship between UPV (V) and concrete compressive strength (f_c') as (Tharmaratnam and Tan 1990):

$$f_c' = ae^{bV} \tag{1}$$

where *a* and *b* are coefficients to be calibrated experimentally, and this relationship was found applicable to concrete with other SCMs such as fly ash and blast furnace slag (Demirboga *et al.* 2004). A similar exponential relationship between the ultrasonic pulse velocity and compressive strength can be established for LC3 concretes. Based on the experimental results obtained, Equation 1 has been successfully calibrated for LC3 concrete (**Fig. 7**).

Figure 8 presents the pore size distribution obtained for all cement pastes using mercury intrusion po-

rosimetry (MIP). This technique is based on simple principle of mercury intrusion into porous structure with increasing pressure (Scrivener *et al.* 2016). However, there are some limitations in MIP data interpretation due to the model assumption. Firstly, the pore size calculation is assumed based on Washburn equation for cylindrical pores. However, pore shape in cement system is not cylindrical, as demonstrated by scanning electron microscopy (SEM) (Diamond 2000). Secondly, isolated pores are not intruded by MIP technique. Thus, MIP data only exhibited the porosity of interconnected and accessible pores. Lastly, MIP experiment only measures the pore size entry instead of pore volume, knowns as ink-bottle effect, which can result in errors on the pore size volume measurement with increasing small pores and decreasing large pores (Lange *et al*. 1994; Scrivener *et al*. 2016). Due to these limitations, MIP data shows only the volume of pore entry size within interconnected and accessible pores. Nevertheless, MIP technique provides a reliable comparison of pore structures of cementitious materials by utilizing the same experimental parameter including drying process, surface tension and contact angle of mercury, pressurisation rate, sample

mass and number of specimens. MIP experiment has also been widely-accepted for investigating pore structure of cementitious blended systems including LC3-based system (Berodier and Scrivener 2015; Dhandapani and Santhanam 2017; Tironi *et al*. 2017).

Calcined clay and limestone can contribute to reducing the quantity of pores bigger than 0.1μm in comparison with GP cement pastes (GPC-50 and GPC-30). A similar reduction in coarse pores content was reported in a previous study as well (Tironi *et al*. 2017)**.** For small pores less than 0.01 μm, GPC-30 showed the highest quantity, followed by LC3-45 paste. A similar porosity in the fine pore range was exhibited by GPC-50 and LC3-30 while LC3-15 specimen obtained the lowest amount of pores smaller than 0.01 μm. Noticeably, among concrete containing calcined clay and limestone (LC3-15, LC3-30 and LC3-45), the increase in GP cement substitution resulted in increasing the quantity of pores less than 0.01 μm diameter and decreasing the quantity of pores more than 0.1 μm diameter.

The total percolated pore volume (total porosity) of GP cement and LC3 pastes is also presented in **Fig. 8** and is calculated as the maximum pore volume (acces-
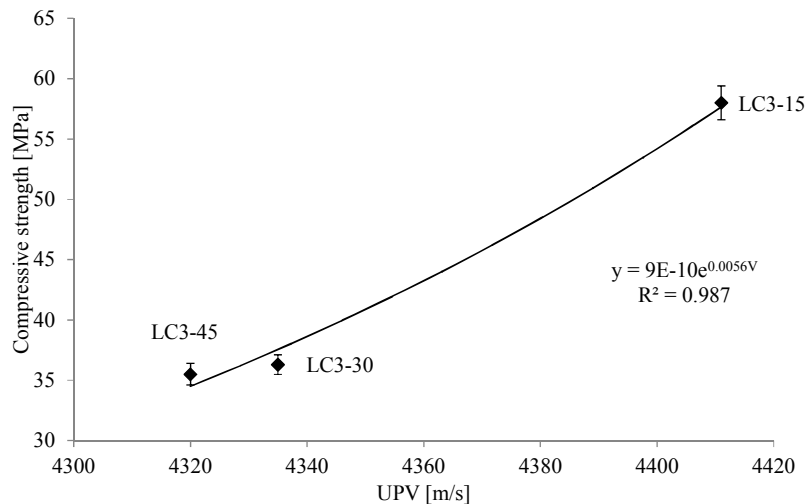

Fig. 7 Relationship between ultrasonic pulse velocity and compressive strength of LC3 concretes at 28 days.
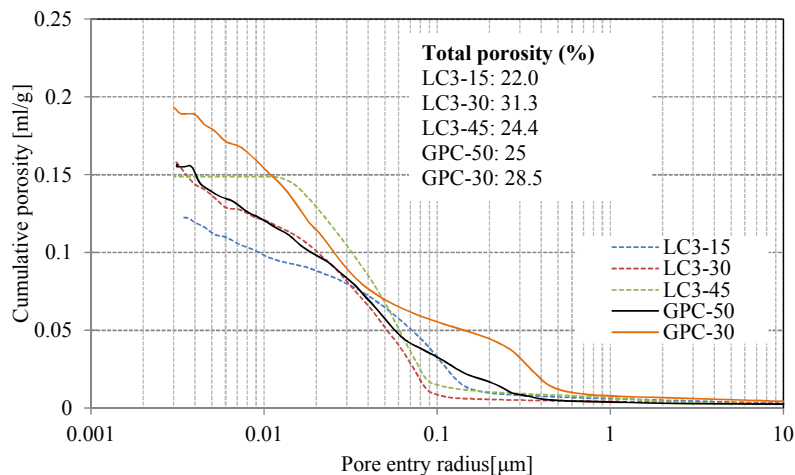

Fig. 8 Pore structure distribution by mercury intrusion porosimetry (MIP).

sible or percolated pores) intruded throughout MIP experiment over total sample volume. Total porosity of LC3-15 is the lowest obtained, which is consistent with its high compressive strength and UPV values. The total porosity of LC3-45 specimens (24.4%) is smaller than that of LC-30 and GPC-30 which is the only porosity test result not consistent with compressive strength results. However, the average pore size of LC3-45 was higher than all other concrete tested (**Fig. 12**). The average pore size is determined as following:

$$Average\ pore\ size = \frac{4 \times V_{tot}}{A_{tot}} \tag{2}$$

where V_{tot} is the total intrusion volume in the sample (ml/g) and A_{tot} is the total calculated areas of pores (m^2/g).

Table 8 shows that the surface resistivity increases significantly with the increasing replacement of GP cement by limestone and calcined clay. The lowest value was 19.4 kΩ.cm belonging to GPC-50 and the highest value was 78.9 kΩ.cm obtained by LC3-45. Previous study (Polder 2001) highlighted that concrete resistivity is correlated to the risk of steel reinforcement corrosion. In general, the higher the surface resistivity, the lower the corrosion rate. Moreover, low chloride diffusion coefficients were obtained in concrete with high resistivity (Andrade et al. 1994; Polder 2001). Therefore, LC3-based concrete has the potential of having a high resistance against chloride induced steel corrosion. A study is currently in progress at UNSW Sydney aiming to assess chloride induced steel corrosion in LC3 concrete. It is also interesting to notice that the surface resistivity shows an opposite trend compared to compressive strength, while some previous studies showed a similar trend (Khan et al. 2016; Noushini and Castel 2016; Ramezanianpour et al. 2011).

Resistivity is usually considered closely related to interconnected void and moisture content in the pore network. However, the resistivity of concrete depends as well on ions movement in the pore solution. High ions concentration in the pore solution leads to a reduction in concrete resistivity (Noushini and Castel 2016; Palacky 1988; Shi et al. 1998). The correlation between surface resistivity and ions concentration in the pore solution is shown in **Fig. 9**. The coefficient of determination R^2 over 0.95 indicates a good correlation between surface resistivity and ions concentration. On the contrary, the concrete surface resistivity is poorly correlated to the concrete total porosity as shown in **Fig. 10** with an extremely low R^2 = 0.04. Consequently, it is obvious that the surface resistivity is predominantly governed by the ion concentration in the pore solution of the concrete.

Regarding the bulk density, the highest and lowest bulk density were 2.25 T/m^3 and 2.18 T/m^3 obtained for GPC-50 and LC3-45 concretes respectively. This result indicates that using calcined clay and limestone does not impact the bulk density of concrete.

3.6 Drying shrinkage

Drying shrinkage was measured according to Australian Standard AS 1012.13 recommendations. Drying shrinkage test starts on the seventh day. It is assumed that, at this stage, a large part of the autogenous shrinkage has already happened. As a result, AS 1012.13 procedure allows measuring drying shrinkage only. Results are presented in **Fig. 11** for all concretes up to 56 days. Overall, LC3 specimens show higher 56 days drying shrinkage than reference GP cement concretes. At 56 days, the highest shrinkage strain was measured on LC3-45 with about 750 microstrains, then LC3-15 samples obtained the second highest magnitude with 720 microstrains. Drying shrinkage of GPC-50, GPC-30 and LC3-30 mixes developed gradually and reached about 550,600 and 650 microstrains after 56 days, respectively.

The higher volume and size of capillary pores communicating to concrete surface encourages water to diffuse and evaporate in the environment leading to higher drying shrinkage. Brook et al. (Brooks and Johari 2001) indicated that OPC cement replacement by calcined clay could reduce the magnitude of drying shrinkage in concrete for a period of 200 days whereas higher drying
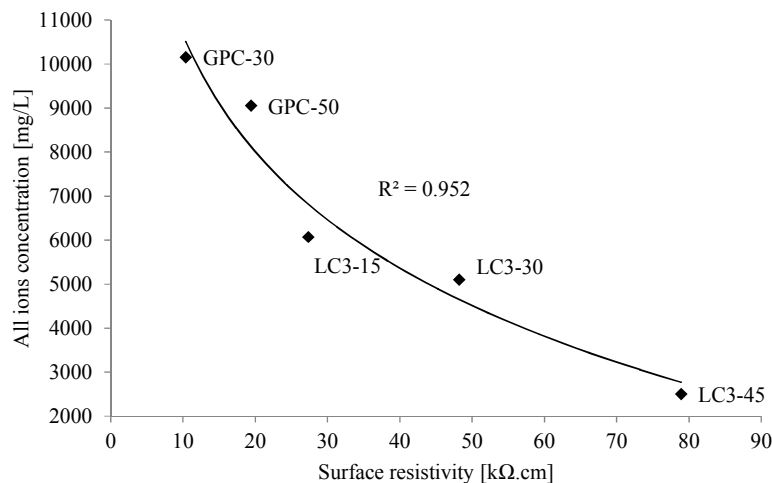

Fig. 9 Relationship between surface resistivity and all ions concentration in pore solution at 28 days.

shrinkage than reference concrete was reported by Valcuende (Valcuende *et al.* 2012) in blends with limestone filler. In this study, combining calcined clay and limestone led to an increase in drying shrinkage compared to reference concretes which can be linked to the higher average pore size of LC3 pastes measured using MIP (**Fig. 12**). As shrinkage test starts 7 days after batching, another possible explanation is that LC3 concretes undergo more autogenous shrinkage compared to GP cement concretes between 7 and 56 days. Further investigations are in progress to confirm this statement.

4. Conclusions

This study aimed to assess various engineering properties of both fresh and hardened limestone calcined clay concrete. Limestone and calcined clay blend is used as any other supplementary cementitious material in Australia by straight replacement of General Purpose cement without any optimisation of sulphate content or alkalinity. This approach aims to reduce the time for limestone and calcined clay blend adoption in the industry. The following conclusions can be drawn.

(1) XRD results showed a reduction in Portlandite formed in limestone calcined clay concrete due to the pozzolanic reactions and the reduction in General Purpose cement content in the mix. The quantity of calcite and hermicarboaluminate phases observed increased proportionately with the GP cement substitution rate.

(2) A reduction in concrete workability was observed with the increase in General Purpose cement substitution. Superplasticiser was required to obtain a slump equivalent to that of reference concrete.

(3) The 28 days average compressive strength of LC3-15 concrete with 15% substitution was higher than that of reference concrete GPC-50. However, for 30% and 45% GP cement substitution by low grade calcined clay and limestone, the 28-day compressive strength of limestone calcined clay concretes was significantly lower, ranging between 35.5 MPa and 36.3 MPa. Considering concretes with similar 28-day compressive strength, results showed that the 7-day compressive strength was only marginally af-
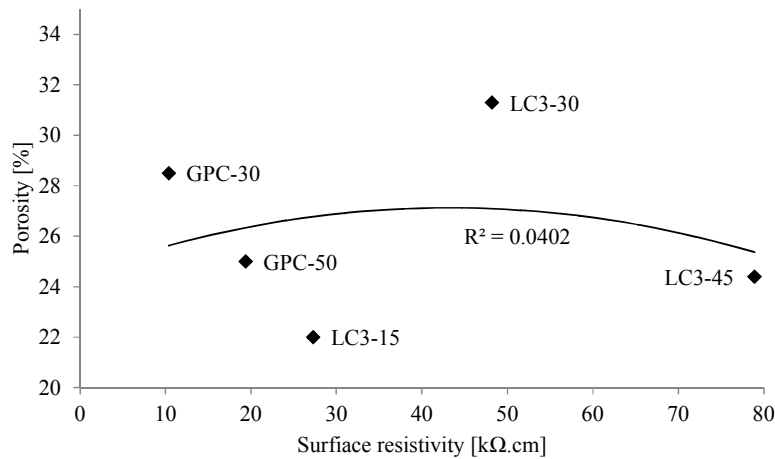

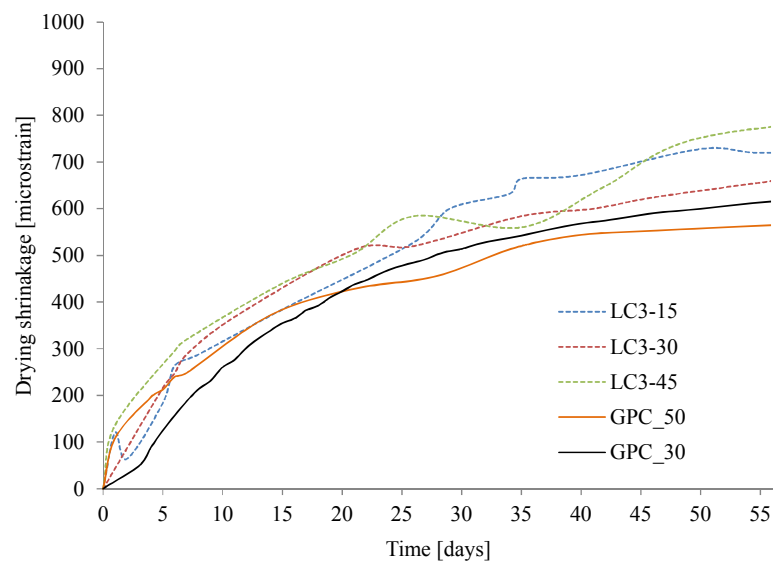Fig. 10 Relationship between surface resistivity and porosity at 28 days.
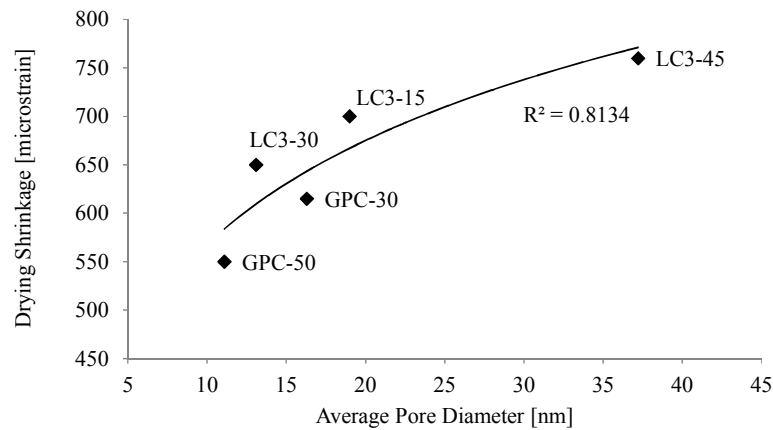

Fig. 11 Drying shrinkage of concretes.

Fig. 12. Relationship between drying shrinkage at 56 days and average pore diameter from MIP results.

fected by the limestone and calcined clay substitution.

(4) The surface resistivity of limestone calcined clay concretes was remarkably higher than that of reference concretes. The higher electrical resistivity of limestone calcined clay concrete may reflect a better chloride-induced reinforcement corrosion resistance. Further investigations are in progress to confirm this statement. Drying shrinkage of limestone calcined clay concrete was slightly higher than that of reference General Purpose cement concretes.

(5) Mercury Intrusion Porosimetry results revealed that using calcined clay and limestone contributed to increase the quantity of pores inferior to 0.01 μm and reduce the quantity of coarser pores (with size > 0.1 μm).

References

Ambroise, J., Maximilien, S. and Pera, J., (1994). "Properties of metakaolin blended cements." *Advanced Cement Based Materials*, 1(4), 161-168.

Andrade, C., Sanjuan, M. A., Recuero, A. and Rio, O., (1994). "Calculation of chloride diffusivity in concrete from migration experiments, in Non-Steady-State Conditions." *Cement and Concrete Research*, 24(7), 1214-1228.

Antoni, M., (2013). "*Investigation of cement substitution by blends of calcined clays and limestone.*" Thesis (PhD), Swiss Federal Institute of Technology in Lausanne.

Antoni, M., Rossen, J., Martirena, F. and Scrivener, K., (2012). "Cement substitution by a combination of metakaolin and limestone." *Cement and Concrete Research*, 42(12), 1579-1589.

Badogiannis, E., Kakali, G., Dimopoulou, G., Chaniotakis, E. and Tsivilis, S., (2005). "Metakaolin as a main cement constituent. Exploitation of poor Greek kaolins." *Cement and Concrete Composites*, 27(2), 197-203.

Badogiannis, E., Papadakis, V., Chaniotakis, E. and Tsivilis, S., (2004). "Exploitation of poor Greek kaolins: strength development of metakaolin concrete and evaluation by means of k-value." *Cement and Concrete Research*, 34(6), 1035-1041.

Badogiannis, E. and Tsivilis, S., (2009). "Exploitation of poor Greek kaolins: Durability of metakaolin concrete." *Cement Concrete Composites*, 31(2), 128-133.

Barneyback, R. S. and Diamond, S., (1981). "Expression and analysis of pore fluids from hardened cement pastes and mortars." *Cement and Concrete Research*, 11(2), 279-285.

Berodier, E. and Scrivener, K., (2015). "Evolution of pore structure in blended systems." *Cement and Concrete Research*, 73, 25-35.

Bonavetti, V., Donza, H., Rahhal, V. and Irassar, E., (2000). "Influence of initial curing on the properties of concrete containing limestone blended cement." *Cement and Concrete Research*, 30(5), 703-708.

Bosiljkov, V. B., (2003). "SCC mixes with poorly graded aggregate and high volume of limestone filler." *Cement and Concrete Research*, 33(9), 1279-1286.

Brooks, J. J. and Johari, M. A. M., (2001). "Effect of metakaolin on creep and shrinkage of concrete." *Cement Concrete Composites*, 23(6), 495-502.

Cassagnabere, F., Diederich, P., Mouret, M., Escadeillas, G. and Lachemi, M., (2013). "Impact of metakaolin characteristics on the rheological properties of mortar in the fresh state." *Cement Concrete Composites*, 37, 95-107.

Damtoft, J. S., Lukasik, J., Herfort, D., Sorrentino, D. and Gartner, E. M., (2008). "Sustainable development and climate change initiatives." *Cement and Concrete Research*, 38(2), 115-127.

De Weerdt, K., Kjellsen, K., Sellevold, E. and Justnes, H., (2011). "Synergy between fly ash and limestone

powder in ternary cements." *Cement and Concrete Composites*, 33(1), 30-38.

Demirboga, R., Turkmen, I. and Karakoc, M. B., (2004). "Relationship between ultrasonic velocity and compressive strength for high-volume mineral-admixtured concrete." *Cement and Concrete Research*, 34(12), 2329-2336.

Dhandapani, Y. and Santhanam, M., (2017). "Assessment of pore structure evolution in the limestone calcined clay cementitious system and its implications for performance." *Cement Concrete Composites*, 84, 36-47.

Diamond, S., (2000). "Mercury porosimetry - An inappropriate method for the measurement of pore size distributions in cement-based materials." *Cement and Concrete Research*, 30(10), 1517-1525.

He, C., Osbaeck, B. and Makovicky, E., (1995). "Pozzolanic reactions of six principal clay minerals: activation, reactivity assessments and technological effects." *Cement and Concrete Research*, 25(8), 1691-1702.

Ipavec, A., Gabrovšek, R., Vuk, T., Kaučič, V., Maček, J. and Meden, A., (2011). "Carboaluminate phases formation during the hydration of calcite-containing portland cement." *Journal of the American Ceramic Society*, 94(4), 1238-1242.

Justice, J. and Kurtis, K., (2007). "Influence of metakaolin surface area on properties of cement-based materials." *Journal of Materials in Civil Engineering*, 19(9), 762-771.

Khan, M. S. H., Castel, A., Akbarnezhad, A., Foster, S. J. and Smith, M., (2016). "Utilisation of steel furnace slag coarse aggregate in a low calcium fly ash geopolymer concrete." *Cement and Concrete Research*, 89, 220-229.

Khan, M. S. H., Nguyen, Q. D. and Castel, A., (2018). "Carbonation of limestone calcined clay cement concrete." in: Martirena, F., Favier, A., Scrivener, K., Eds. *Proc. of the 2nd International Conference on Calcined Clay for Sustainable Concrete*, Springer Netherlands, 238-243.

Khatib, J. and Hibbert, J., (2005). "Selected engineering properties of concrete incorporating slag and metakaolin." *Construction and Building Materials*, 19(6), 460-472.

Kim, T., Olek, J. and Jeong, H., (2015). "Alkali-silica reaction: Kinetics of chemistry of pore solution and calcium hydroxide content in cementitious system." *Cement and Concrete Research*, 71(Supplement C), 36-45.

Kumar, A., Oey, T., Falla, G. P., Henkensiefken, R., Neithalath, N. and Sant, G., (2013a). "A comparison of intergrinding and blending limestone on reaction and strength evolution in cementitious materials." *Construction and Building Materials*, 43 (Supplement C), 428-435.

Kumar, A., Oey, T., Kim, S., Thomas, D., Badran, S., Li, J. L., Fernandes, F., Neithalath, N. and Sant, G.,

(2013b). "Simple methods to estimate the influence of limestone fillers on reaction and property evolution in cementitious materials." *Cement Concrete Composites*, 42 (Supplement C), 20-29.

Kunther, W., Dai, Z. and Skibsted, J., (2016). "Thermodynamic modeling of hydrated white Portland cement-metakaolin-limestone blends utilizing hydration kinetics from Si-29 MAS NMR spectroscopy." *Cement and Concrete Research*, 86, 29-41.

Lange, D. A., Jennings, H. M. and Shah, S. P., (1994). "Image-Analysis Techniques for characterization of pore structure of cement-based materials." *Cement and Concrete Research*, 24(5), 841-853.

Lin, Y., Lai, C.-P. and Yen, T., (2003). "Prediction of ultrasonic pulse velocity (UPV) in concrete." *Materials Journal*, 100(1), 21-28.

Lothenbach, B., Scrivener, K. and Hooton, R. D., (2011). "Supplementary cementitious materials." *Cement and Concrete Research*, 41(12), 1244-1256.

Matschei, T., Lothenbach, B. and Glasser, F. P., (2007). "The AFm phase in portland cement." *Cement and Concrete Research*, 37(2), 118-130.

Menendez, G., Bonavetti, V. and Irassar, E. F., (2003). "Strength development of ternary blended cement with limestone filler and blast-furnace slag." *Cement Concrete Composites*, 25(1), 61-67.

Mounanga, P., Khokhar, M. I. A., El Hachem, R. and Loukili, A., (2011). "Improvement of the early-age reactivity of fly ash and blast furnace slag cementitious systems using limestone filler." *Materials and Structures*, 44(2), 437-453.

Neville, A. M., (1995). "*Properties of concrete*." Pearson Education Limited.

Noushini, A. and Castel, A., (2016). "The effect of heat-curing on transport properties of low-calcium fly ash-based geopolymer concrete." *Construction and Building Materials*, 112, 464-477.

Oey, T., Kumar, A., Bullard, J. W., Neithalath, N. and Sant, G., (2013). "The filler effect: The influence of filler content and curface area on cementitious reaction rates." *Journal of the American Ceramic Society*, 96(6), 1978-1990.

Palacky, G., (1988) "Resistivity characteristics of geologic targets." in: Nabighion, M., Ed. *Electromagnetic Methods in Applied Geophysics-Theory*, Society of Exploration Geophysicist Tulsa, 53-130.

Polder, R. B., (2001). "Test methods for on site measurement of resistivity of concrete - a RILEM TC-154 technical recommendation." *Construction and Building Materials*, 15(2), 125-131.

Puerta-Falla, G., Balonis, M., Le Saout, G., Falzone, G., Zhang, C., Neithalath, N. and Sant, G., (2015a). "Elucidating the role of the aluminous source on limestone reactivity in cementitious materials." *Journal of the American Ceramic Society*, 98(12), 4076-4089.

Puerta-Falla, G., Balonis, M., Le Saout, G., Kumar, A., Rivera, M., Falzone, G., Neithalath, N. and Sant, G.,

(2016). "The influence of slightly and highly soluble carbonate salts on phase relations in hydrated calcium aluminate cements." *Journal of Materials Science*, 51(12), 6062-6074.

Puerta-Falla, G., Balonis, M., Le Saout, G., Neithalath, N. and Sant, G., (2015b). "The influence of metakaolin on limestone reactivity in cementitious materials." in: K. Scrivener, and A. Favier, Eds. *Calcined Clays for Sustainable Concrete: Proceedings of the 1st International Conference on Calcined Clays for Sustainable Concrete*, Springer Netherlands, Dordrecht, 11-19.

Qian, X. and Li, Z., (2001). "The relationships between stress and strain for high-performance concrete with metakaolin." *Cement and Concrete Research*, 31(11), 1607-1611.

Ramezanianpour, A. A., (2014). "*Metakaolin.*" Springer.

Ramezanianpour, A. A., Pilvar, A., Mandikhani, M. and Moodi, F., (2011). "Practical evaluation of relationship between concrete resistivity, water penetration, rapid chloride penetration and compressive strength." *Construction and Building Materials*, 25(5), 2472-2479.

San Nicolas, R., Cyr, M. and Escadeillas, G., (2013). "Characteristics and applications of flash metakaolins." *Applied Clay Science*, 83, 253-262.

San Nicolas, R., Cyr, M. and Escadeillas, G., (2014). "Performance-based approach to durability of concrete containing flash-calcined metakaolin as cement replacement." *Construction and Building Materials*, 55, 313-322.

Scrivener, K., Snellings, R. and Lothenbach, B., (2016). *A practical guide to microstructural analysis of cementitious materials*, CRC Press.

Shi, C., Stegemann, J. A. and Caldwell, R. J., (1998). "Effect of supplementary cementing materials on the specific conductivity of pore solution and its implications on the rapid chloride permeability test (AASHTO T277 and ASTM C1202) results." *ACI Materials Journal*, 95(4), 389-394.

Shi, Z. G., Geiker, M. R., Lothenbach, B., De Weerdt, K., Garzon, S. F., Enemark-Rasmussen, K. and Skibsted, J., (2017). "Friedel's salt profiles from thermogravimetric analysis and thermodynamic modelling of Portland cement-based mortars exposed to sodium chloride solution." *Cement Concrete Composites*, 78, 73-83.

Shi, Z. G., Lothenbach, B., Geiker, M. R., Kaufmann, J., Leemann, A., Ferreiro, S. and Skibsted, J., (2016). "Experimental studies and thermodynamic modeling of the carbonation of Portland cement, metakaolin and limestone mortars." *Cement and Concrete Research*, 88, 60-72.

Siddique, R. and Klaus, J., (2009). "Influence of metakaolin on the properties of mortar and concrete: A review." *Applied Clay Science*, 43(3-4), 392-400.

Sturrup, V., Vecchio, F. and Caratin, H., (1984). "Pulse velocity as a measure of concrete compressive strength." *Special Publication*, 82, 201-228.

Tharmaratnam, K. and Tan, B. S., (1990). "Attenuation of ultrasonic pulse in cement mortar." *Cement and Concrete Research*, 20(3), 335-345.

Tironi, A., Scian, A. N. and Irassar, E. F., (2017). "Blended cements with limestone filler and kaolinitic calcined clay: Filler and pozzolanic effects." *Journal of Materials in Civil Engineering*, 29(9), 04017116.

Tironi, A., Trezza, M. A., Scian, A. N. and Irassar, E. F., (2012). "Kaolinitic calcined clays: Factors affecting its performance as pozzolans." *Construction and Building Materials*, 28(1), 276-281.

Tironi, A., Trezza, M. A., Scian, A. N. and Irassar, E. F., (2013). "Assessment of pozzolanic activity of different calcined clays." *Cement Concrete Composites*, 37, 319-327.

Valcuende, M., Marco, E., Parra, C. and Serna, P., (2012). "Influence of limestone filler and viscosity-modifying admixture on the shrinkage of self-compacting concrete." *Cement and Concrete Research*, 42(4), 583-592.

Vance, K., Aguayo, M., Oey, T., Sant, G. and Neithalath, N., (2013a). "Hydration and strength development in ternary portland cement blends containing limestone and fly ash or metakaolin." *Cement and Concrete Composites*, 39, 93-103.

Vance, K., Kumar, A., Sant, G. and Neithalath, N., (2013b). "The rheological properties of ternary binders containing Portland cement, limestone, and metakaolin or fly ash." *Cement and Concrete Research*, 52, 196-207.

Vizcaíno Andrés, L. M., Antoni, M. G., Alujas Diaz, A., Martirena Hernández, J. F. and Scrivener, K. L., (2015). "Effect of fineness in clinker-calcined clays-limestone cements." *Advances in Cement Research*, 27(9), 546-556.

Vizcaíno, L., Antoni, M., Alujas, A., Martirena, F. and Scrivener, K., (2015). "Industrial manufacture of a low-clinker blended cement using low-grade calcined clays and limestone as SCM: The cuban experience." in: K. Scrivener, and A. Favier, Eds. *Calcined Clays for Sustainable Concrete: Proceedings of the 1st International Conference on Calcined Clays for Sustainable Concrete*, Springer Netherlands, Dordrecht, 347-358.

Whitehurst, E. A., (1951). "*Soniscope tests concrete structures.*" Chicago, Portland Cement Association.

Wild, S., Khatib, J. M. and Jones, A., (1996). "Relative strength, pozzolanic activity and cement hydration in superplasticised metakaolin concrete." *Cement and Concrete Research*, 26(10), 1537-1544.

Worrell, E., Price, L., Martin, N., Hendriks, C. and Meida, L. O., (2001). "Carbon dioxide emissions from the global cement industry 1." *Annual Review of Energy and the Environment*, 26(1), 303-329.

Zhang, J. and Scherer, G. W., (2011). "Comparison of methods for arresting hydration of cement." *Cement and Concrete Research*, 41(10), 1024-1036.